1. Grzegorz KŁOSOWSKI[3], 2. Przemysław ADAMKIEWICZ [1], 3. Konrad NIDERLA[1,2]

University of Economics and Innovation in Lublin (1), Research and Development Center Netrix S.A. (2),
Lublin University of Technology (3)
1. 0000-0001-7927-3674, 2. 0000-0003-3425-9566, 3. 0000-0003-1280-0622

Combining electrical capacitance and impedance tomography in monitoring processes

Abstract. The presented research describes an experiment aimed at answering the question of whether the combination of two types of tomographic measurements, namely electrical impedance tomography (EIT) and electrical capacitance tomography (ECT), will improve the quality of the reconstruction in comparison to the tomographic images obtained with both methods considered separately. For this purpose, appropriate tests were carried out, which showed that, in fact, magnification of the measurement vector by combining EIT and ECT measurements increases the quality of the reconstruction.

*Streszczenie. W przedstawionych badaniach opisano eksperyment mający za zadanie odpowiedź na pytanie, czy połączenie dwóch rodzajów pomiarów tomograficznych, a mianowicie elektrycznej tomografii impedancyjnej (EIT) i elektrycznej tomografii pojemnościowej (ECT), podniesie jakość rekonstrukcji w porównaniu do obrazów tomograficznych uzyskanych obiema rozpatrywanymi metodami z osobna. W tym celu przeprowadzono stosowne próby, które wykazały, że istotnie, powiększenie wektora pomiarowego poprzez połączenie pomiarów EIT i ECT powoduje wzrost jakości rekonstrukcji. (**Łączenie tomografii elektrycznej pojemnościowej i impedancyjnej w procesach monitorowania**).*

Keywords: machine learning; electrical impedance tomography; electrical capacitance tomography; process tomography; hybrid tomography
Słowa kluczowe: uczenie maszynowe; elektryczna tomografia impedancyjna; tomografia procesowa; tomografia hybrydowa

Introduction

Industrial tomography is a dynamically developing field of technology. Effective control of industrial processes requires constant supervision and monitoring of many parameters at the same time. Based on information flowing into the monitoring system, individual machines, devices, and technical apparatus react to changes in the work environment. The reaction consists in adjusting physical parameters such as temperature, pressure, flow, substrate concentration, etc. [1]. Process control can apply to both discrete technological systems and the production of liquid or gaseous substances. Figure 1 shows an example of an industrial tank reactor. Industrial reactors are designed to maintain optimum economic parameters of chemical operations. This is possible with the right reactor design and the strategic overlap of three different kinds of sub-processes happening within the reactor: the transfer of mass, momentum, and heat.

The first reaction category involves solidifying substances in a liquid medium. It discusses the modifications of particle characteristics and industrial procedures for creating and purifying solids. Crystallization reactors find applications across numerous industries, including the chemical, food, and metalworking sectors [2]. In real-time, monitoring systems must provide accurate data on the number, size, and location of crystals forming in a liquid.

(a)   **(b)**
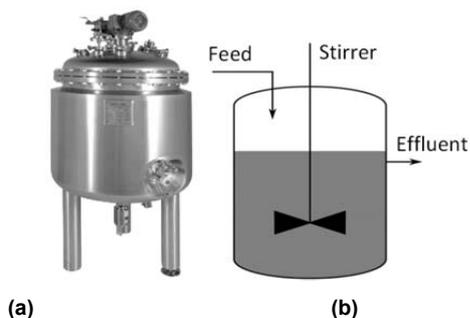
Fig. 1. Continuous stirred-tank reactor: (a) - a real device, (b) – a model

The second kind of reaction is one involving a mixture of gas and liquid. One such use is in the creation of biogas. Biogas plants depend on physicochemical and fermentation reactors. Methane and organic waste are fermented within these reactors. The dependability of industrial operations relies in large part on the efficient functioning of this technological system [3].

There are primarily two goals in keeping tabs on the status of dynamic processes. One is the early warning of imminent failures, such as those caused by a breakdown in the technological infrastructure, an abnormally large change in key process parameters, or a break in the continuity of operations. An efficient monitoring system is built to help find issues before they become catastrophic so that remedial measures may be implemented efficiently. Controlling the track of an industrial process is the second justification for monitoring its states.

Electrical tomography is a non-invasive method that allows visualisation and monitoring changes inside reactors and pipelines [4–6]. The most common types of electrical tomography are electrical impedance tomography (EIT) and electrical capacitance tomography (ECT) [7–10]. The observations and research allowed to formulate the thesis that the optimal selection of the type of tomographic method used (EIT or ECT) depends on many factors, including the type of monitored object and the characteristics of the process. The key attributes of the reactor include its size, material and wall thickness, the chemical composition of the filling substance, and physical parameters such as mixing speed, pressure, and temperature. The basic features of the process include its dynamics, understood as the rate of changes in the state of the tested object, the proportions of substrates, temperature, pressure, and flow rate [11-14].

Materials and Methods

To solve the tomographic inverse problem, consisting in converting measurements into images, a hybrid measurement system was used. This heterogeneous system is a combination of two types of tomography - EIT and ECT. The homogeneous EIT method uses 96 voltage measurements, and the ECT measurement vector consists of 120 capacitance values. We combined both

measurement vectors, and then we got 216 heterogeneous values of voltage and capacitance at the input. The output is an image with a resolution of 4146 pixels (tetrahedron finite elements). Figure 1 shows a diagram of the operation of a hybrid tomographic system combining two types of tomography - EIT and ECT.
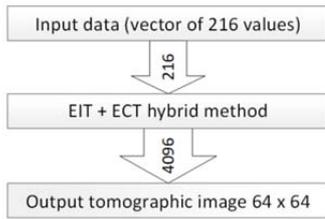
Fig. 2. Model of operation of a hybrid tomographic system combining two types of tomography - EIT and ECT

Figure 3 shows the method of conducting the described research. First, two training sets were simulated. The first set was generated with EIT tomography in mind. The same reference images served as the output models to generate the ECT measurements. Eidors software cooperating with Matlab was used in both cases. The observations were generated by solving a simple problem using the finite element method. In other words, the measurement set for 16 electrodes was calculated for the reference cases defined on the finite element mesh. Since each type of tomography, EIT and ECT, uses 16 electrodes, the total number of electrodes was 32. Then the two training sets (EIT and ECT) were joined together in such a way that the input vector was extended. The outputs, i.e., the reference images, remained the same.
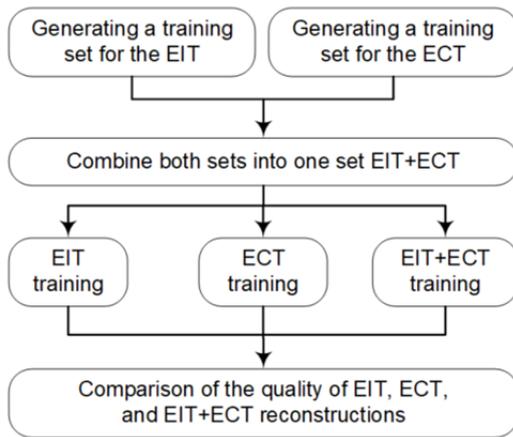
Fig. 3. Workflow of the research
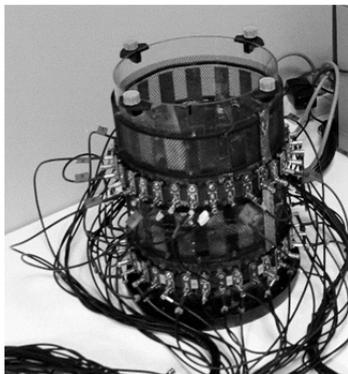
Fig. 4. Measurement tank for imaging real cases

Then, three models of neural networks were trained - two homogeneous ones: the convolutional neural network (CNN) and the long-short-term memory network (LSTM), and one hybrid connecting both networks (CNN+LSTM) [15–17]. All three types of trained models were compared, and it was found that the best results were obtained with a model containing both CNN and LSTM layers.

Figure 4 shows the physical model of the tank with the EIT and ECT electrodes. The presented stand enables the imaging of real measurements using the tested hybrid EIT and ECT measurements.

Figure 5 shows the 11-layer architecture of the CNN network. Since the inputs are a 216-element vector, layer one is sequential.

The next layer is a 1D convolution layer with filterSize = 29 and numFilters = 9 parameters. This is followed by the batch normalization layer which calculates the normalized activations $\hat{x}_i$ of input elements x_i according to formula (1)

(1) $\qquad \hat{x}_i = \frac{x_i - \mu_B}{\sqrt{\sigma_B^2 + \epsilon}}$

where μ_B is mean, and σ_B^2 is variance. Both parameters are calculated over the spatial, time, and case dimensions for each channel individually. Once the variance becomes negligible, numerical stability is improved by the constant ϵ. The activations are further shifted and scaled using the (2) transformation for accounting for the potential that inputs with zero mean and unit variance are not ideal for the processes that follow batch normalization.

(2) $\qquad y_i = \gamma \hat{x}_i + \beta$

The scale factor γ, and offset β and are learnable parameters that are updated during artificial neural network learning.
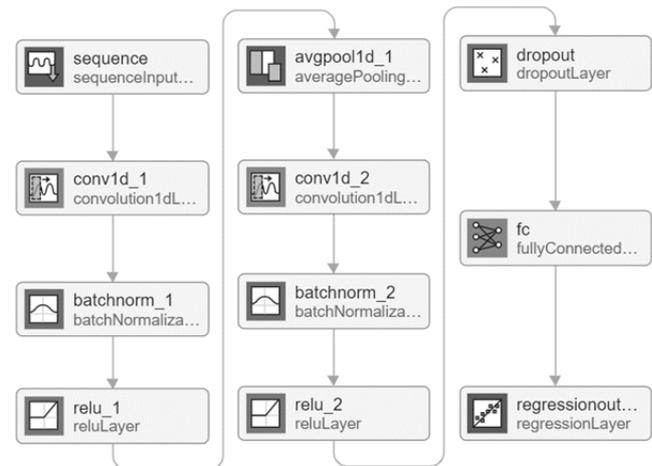
Fig.5. CNN layers used in the hybrid network

Downsampling is carried out via a 1D average pooling layer, which accomplishes this task by first splitting the input into 1D pooling areas and then calculating the average value for each of these regions. The dropout layer is designed to counteract overfitting by randomly setting the input elements to zero with a certain probability. The fully connected layer adds the input and weight products and adds a bias vector. When it comes to regression tasks, the regression layer is responsible for computing the loss of the half-mean squared error. Figure 6 shows the architecture of the LSTM network. The entire network consists of a layer of layers. This is this text to build a site with CNN. The biLSTM and LSTM layers are new.

The bidirectional long short-term memory, or biLSTM, the layer is responsible for the learning of long-term dependencies in both directions between the time steps in a time series or sequence of data. When it wants the network to learn from the whole time series at each time step, these dependencies might be helpful in achieving that goal. Learning the long-term relationships between time steps in time series and sequence data is the responsibility of an LSTM layer. The layer engages in additive interactions, which may assist in enhancing gradient flow over extensive sequences while the network is being trained. The number of hidden units (or the hidden size) is specified as a positive integer.
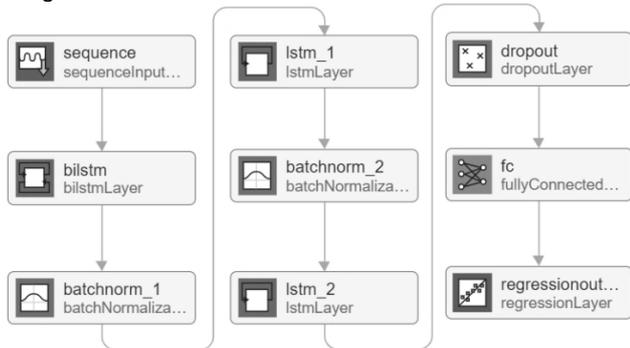
Fig.6. The way of using LSTM layers in the hybrid network

The information retained from one-time step to the next is proportional to the number of hidden units (the hidden state). Regardless of sequence length, information from all preceding time steps may be stored in the hidden state. The layer may overfit its input data if too many hidden units are used. Prices can range from the low hundreds to the low thousands. There is no upper bound on the number of iterations per time step imposed by the hidden state. Figure 7 depicts the CNN + LSTM hybrid network, which consists of 13 layers. The unique feature of this architecture is the fact that it consists of both CNN and LSTM layers.

Results
Figure 8 shows three types of measurement cases that were reconstructed from actual measurements using the CNN + LSTM algorithm. The considered observations refer to single, double, and triple inclusion. The comparison of reconstructions made based on measurements made on a real object does not make it possible to calculate objective (numerical) quality indicators. Figure 9 shows the three measurement cases reconstructed from simulation measurements using the CNN + LSTM algorithm. Figure 9a

shows an example with a small number of inclusions (3 small objects), and Figure 9b shows an observation with lots of hidden objects. Under the reconstruction images, the values of mean square error (MSE) and image correlation coefficient (ICC) indicators are presented. The closer the ICC is to 1, and the closer the MSE is to 0, the better the reconstruction is. It is clearly visible that the EIT + ECT method gives the best results for both small and large numbers of inclusions.
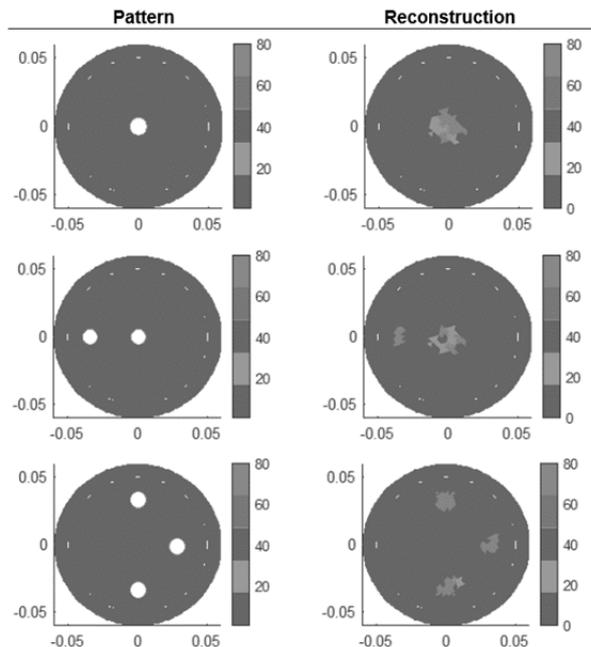
Fig.8. Reconstruction from real measurements with a single, double, and triple inclusion

Conclusions
The research presented in this paper compares the reconstructions of the 2D cross-section of an industrial tank reactor obtained with the use of three methods. The first two methods of tomography are homogeneous, and they are EIT and ECT. The third method used in the research is hybrid (EIT + ECT). Machine learning methods were also compared. The tested algorithms are CNN, LSTM, and the CNN+LSTM hybrid algorithm. At an early stage of the study, the homogeneous CNN and LSTM algorithms were excluded, and all reconstructions were performed with the CNN + LSTM heterogeneous algorithm. Thus, the main focus of research has been focused on the comparative
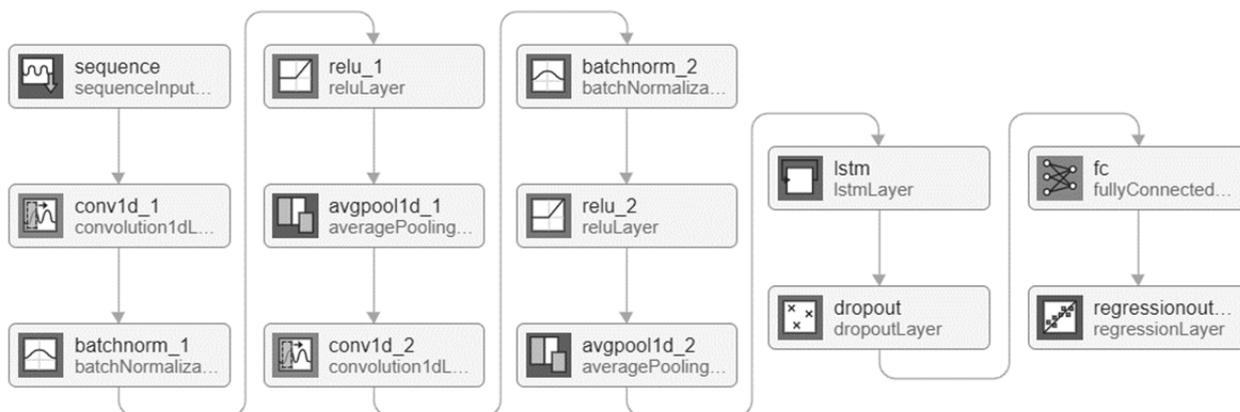
Fig.7. CNN and LSTM layers included in the hybrid artificial neural network

quality

(a)

(b)
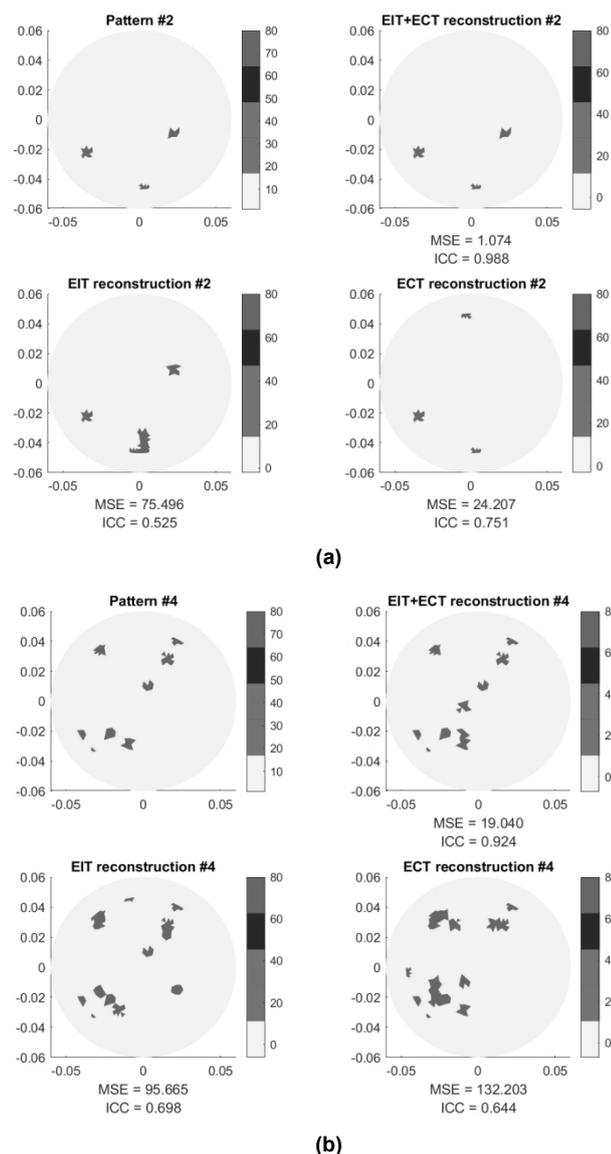
Fig. 9. Reconstructions obtained from simulation-generated measurements: (a) – a few inclusions, (b) – many inclusions

assessment of the three types of electrical tomography, or rather on examining whether the combination of EIT and ECT measurement vectors will increase the quality of the reconstruction. The results of simulation experiments fully confirmed this thesis.

Authors: Grzegorz Kłosowski, Ph.D. Eng., Lublin University of Technology, Nadbystrzycka 38A, Lublin, Poland, E-mail: g.klosowski@pollub.pl; Przemysław Adamkiewicz, Ph.D., University of Economics and Innovation, Projektowa 4, Lublin, Poland, E-mail: przemysław.adamkiewicz@wsei.lublin.pl; Konrad Niderla, M.Sc. Eng., University of Economics and Innovation, Projektowa 4, Lublin, Poland, E-mail: konrad.niderla@wsei.lublin.pl

REFERENCES

[1] Kłosowski G., Rymarczyk T., Kania K., Świć A., Cieplak T., Maintenance of industrial reactors supported by deep learning driven ultrasound tomography, Eksploatacja i Niezawodnosc – Maintenance and Reliability; 22 (2020), No 1, 138–147.
[2] Rymarczyk T., Niderla K. Kozłowski E. Król K., Wyrwisz J. Skrzypek-Ahmed S., Gołąbek P., Logistic Regression with Wave Preprocessing to Solve Inverse Problem in Industrial Tomography for Technological Process Control, Energies, 14(2021), No. 23, 8116.
[3] Tian, G.; Yang, B.; Dong, M.; Zhu, R.; Yin, F.; Zhao, X.; Wang, Y.; Xiao, W.; Wang, Q.; Zhang, W.; et al. The Effect of Temperature on the Microbial Communities of Peak Biogas Production in Batch Biogas Reactors. Renew Energy, 123 (2018), 15–25, doi:10.1016/J.RENENE.2018.01.119.
[4] Korzeniewska, E., Krawczyk, A., Mróz, J., Wyszyńska, E., Zawiślak, R., Applications of smart textiles in post-stroke rehabilitation, Sensors (Switzerland), 20 (2020), No. 8, 2370.
[5] Wang, M. Industrial Tomography: Systems and Applications; Elsevier Ltd., Ed.; Woodhead Publishing, (2015); ISBN 9781782421184.
[6] Nordin, N.; Idroas, M.; Zakaria, Z.; Ibrahim, M.N. Tomographic Image Reconstruction of Monitoring Flaws on Gas Pipeline Based on Reverse Ultrasonic Tomography. In Proceedings of the 2014 5th International Conference on Intelligent and Advanced Systems (ICIAS); IEEE, June (2014); 1–6.
[7] Rymarczyk, T.; Kłosowski, G.; Hoła, A.; Sikora, J.; Wołowiec, T.; Tchórzewski, P.; Skowron, S. Comparison of Machine Learning Methods in Electrical Tomography for Detecting Moisture in Building Walls. Energies (Basel) (2021), (2021), 2777, doi:10.3390/en14102777.
[8] Rymarczyk, T.; Kozłowski, E.; Kłosowski, G. Electrical Impedance Tomography in 3D Flood Embankments Testing – Elastic Net Approach. Transactions of the Institute of Measurement and Control, 42 (2019), 680–690, doi:10.1177/0142331219857374.
[9] Kania K., Rymarczyk T., Mazurek M., Skrzypek-Ahmed S., Guzik M., Oleszczuk P., Optimisation of Technological Processes by Solving Inverse Problem through Block-Wise-Transform-Reduction Method Using Open Architecture Sensor Platform, Energies, 14 (2021), No. 24, 8295.
[10] Kozlowski, E.; Rymarczyk, T.; Cieplak, T.; Klosowski, G.; Tchorzewski, P. Application of Logistic Regression to Image Reconstruction in EIT. In Proceedings of the 2019 International Interdisciplinary PhD Workshop (IIPhDW 2019); (2019); 80–83.
[11] Koulountzios P., Aghajanian S., Rymarczyk T., Koiranen T., Soleimani M., An Ultrasound Tomography Method for Monitoring CO2 Capture Process Involving Stirring and CaCO3 Precipitation, Sensors, 21 (2021), No. 21, 6995.
[12] Kania, W., Wajman, R., Ckript: a new scripting language for web applications, Informatyka, Automatyka, Pomiary W Gospodarce I Ochronie Środowiska, 12(2022), No. 2, 4-9.
[13] Styła, M., Adamkiewicz, P., Hybrid navigation system for indoor use. Informatyka, Automatyka, Pomiary W Gospodarce I Ochronie Środowiska, 12 (2022), No. 1, 10-14.
[14] Korzeniewska, E., Sekulska-Nalewajko, J., Gocawski, J., Drożdż, T., Kiebasa, P., Analysis of changes in fruit tissue after the pulsed electric field treatment using optical coherence tomography, EPJ Applied Physics, 91 (2020), No. 3, 30902.
[15] Fabijańska, A.; Banasiak, R. Graph Convolutional Networks for Enhanced Resolution 3D Electrical Capacitance Tomography Image Reconstruction. Appl Soft Comput (2021), 110, 107608, doi:10.1016/J.ASOC.2021.107608.
[16] Yuen, B.; Dong, X.; Lu, T. Inter-Patient CNN-LSTM for QRS Complex Detection in Noisy ECG Signals. IEEE Access, 7 (2019), 169359–169370, doi:10.1109/ACCESS.2019.2955738.
[17] Rymarczyk T., Kłosowski G., Hoła A., Hoła J., Sikora J., Tchórzewski P., Skowron Ł., Historical Buildings Dampness Analysis Using Electrical Tomography and Machine Learning Algorithms, Energies, 14 (2021), No. 5, 1307.